OPTIMAL PMU PLACEMENT AND SIGNAL SELECTION FOR MONITORING CRITICAL POWER SYSTEM OSCILLATIONS

A Thesis

by

TONG HUANG

Submitted to the Office of Graduate and Professional Studies of
Texas A&M University
in partial fulfillment of the requirements for the degree of

MASTER OF SCIENCE

Chair of Committee,	Le Xie
Committee Members,	Garng M. Huang
	Jianhua Huang
	I-Hong Hou
Head of Department,	Miroslav M. Begovic

May 2017

Major Subject: Electrical Engineering

ABSTRACT

In this thesis, a strategy for phasor measurement unit (PMU) optimal placement and signal selection is proposed for monitoring critical oscillations in electric power systems. A robust indicator, mode in output proportion factor (MOPF), is introduced for identify critical PMU locations and signal channels, in order to better monitor power system oscillations with specific oscillation modes. Based on the proposed MOPF, a two-layer algorithm is presented. This algorithm could benefit system operators and planners in the following two ways: 1) it identifies existing PMU devices and signal channels, which provides the best observability for critical oscillation modes; 2) it suggests optimal locations for further PMU deployments, in order to enhance the observability for critical oscillation modes. The performance of proposed algorithm is illustrated via a modified 16-machine-68-bus system and NPCC-140-bus system. Based on the proposed algorithm, all modes of interest can be observed sufficiently under various disturbances. Therefore, the proposed algorithm can be applied to prioritize or deploy PMUs to observe critical oscillation modes in power systems.

DEDICATION

To my parents.

ACKNOWLEDGMENTS

I would like to thank Prof. Le Xie for his encouragement through my research and his suggestions for my life. I am also grateful to Prof. Garng M. Huang for the courses that he offered, because through his courses, I have learned how to learn, that is, keeping asking intelligent questions and answering them by simple examples. Special thanks to all of my committee members for their suggestions on my research, which greatly enriches this work. Finally, I would like to thank my parents for their support and encouragement.

CONTRIBUTORS AND FUNDING SOURCES

Contributors

This work was supported by a thesis committee consisting of Professor Le Xie [advisor], Professor Garng M. Huang and Professor I-hong Hou of the Department of Electrical and Computer Engineering and Professor Jianhua Huang of the Department of Statistics. All work conducted for the thesis was completed by the student independently.

Funding Sources

There are no outside funding contributions to acknowledge related to the research and compilation of this document.

NOMENCLATURE

PMU	Phasor Measurement Unit
PF	Participation Factor
GM	Geometric Measure
MOPF	Mode in Output Proportion Factor
PSD	Power Spectrum Density
FFT	Fast Fourier Transform
WAMPAC	Wide-area Monitoring, Protection and Control
SCADA	Supervisory Control and Data Acquisition
AME	Ambient Modal Estimation
MPC	Modal Power Contribution

TABLE OF CONTENTS

Page

ABSTRACT ii

DEDICATION iii

ACKNOWLEDGMENTS iv

CONTRIBUTORS AND FUNDING SOURCES. v

NOMENCLATURE vi

TABLE OF CONTENTS vii

LIST OF FIGURES ix

LIST OF TABLES x

1. INTRODUCTION AND LITERATURE REVIEW 1

2. DECOMPOSITION OF PMU MEASUREMENTS INTO VARIOUS MODES . 4

3. PROPOSED INDICATOR AND ALGORITHM FOR OBSERVING MODES OF INTEREST 9

3.1 Mode in Output Proportion Factor (MOPF) 9
3.2 Comparison with Existing Concepts 11
3.3 Threshold Selection for Dominant Complex Mode in Given Measurement 13
3.4 Hierarchical Scheme for Optimal PMU Placement and Signal Selection . 13

4. CASE STUDIES 17

4.1 Results of Two-layer Algorithm and Its Validation for the 68-bus System . 17
4.1.1 68-Bus System Description 17
4.1.2 Results for the Two-layer Algorithm 18
4.1.3 PSD Validation 19
4.2 Results of Two-layer Algorithm and Its Validation for the NPCC 140-bus System 20
4.3 Convergence Test of MOPF 21

4.4 Impact of Uncertain Disturbance on Proportion of Complex Modes in Measurements 24
4.5 Comparison with Geometric Measure 26
4.6 Robustness Test 27

5. CONCLUSION 29

REFERENCES 30

APPENDIX A. DERIVATION OF MODE IN OUTPUT PROPORTION IN STATISTICAL WAY 33

LIST OF FIGURES

FIGURE Page

4.1 68-bus test system: numbers of buses equipping with PMU are boxed; the geographic locations of each selected channel in Table 4.1 are marked . . 18

4.2 PSD of selected signals for 68-bus system in Table 4.1. The marked peaks indivate all 5 modes of interest are excited. 20

4.3 PSD of selected signals for NPCC 140-bus system in Table 4.2. 22

4.4 The variation of $p_{262,183}$ (solid line), $p_{201,189}$ (dash-dot line), $p_{195,181}$ (dash line), $p_{260,193}$ (dot line) and $p_{261,207}$ (dash-circle line) in MOPF matrix . . 23

4.5 The evolution of e_a^{τ} (solid line) and e_m^{τ} (dash line). 24

4.6 PSD of real power from bus 36 to 37 (left) and real power from bus 65 to 37 (right) under disturbance $\boldsymbol{u}_1$ (dot line) and $\boldsymbol{u}_2$ (solid line) in the 68-bus system. 25

4.7 Discrepancy between MOPF (solid line) and GM (dash-dot line) of meter measuring reactive power from bus 1 to 2. 26

4.8 PSD of reactive power from bus 1 to 2 (solid line) and real power from bus 39 to 44 (dash-dot line). 27

4.9 Visualization of $r_i^{\bar{\mathcal{C}}}$ for the 68-bus system. 28

LIST OF TABLES

TABLE Page

4.1 Result of Two-layer Algorithm for 68-bus System 19

4.2 Result of Two-layer Algorithm for the NPCC 140-bus System 21

1. INTRODUCTION AND LITERATURE REVIEW[1]

Phasor measurement units (PMU) offer time-stamped measurements with high sampling rate and consequently are considered as a significant role for improving wide-area monitoring, protection and control (WAMPAC) in the future grid [1]. One key advantage of PMU systems compared with the traditional supervisory control and data acquisition (SCADA) systems is that, PMU systems can be applied to real-time monitoring of electromechanical oscillations, thanks to the high sampling rates of PMUs. However, these oscillations cannot be monitored clearly through SCADA systems, since SCADA systems can only provide quasi-steady-state information of the power grid [2]. Comparing with damped oscillations, sustained oscillations draw more attention of system operators, since it indicates stability issues of the system, therefore corrective actions need be taken once they are observed. However, it is common that some oscillation modes could only be monitored clearly through several critical PMU devices and signal channels, due to the uneven distribution of modal information among various measurements [3], [4]. Therefore, one natural question from the perspective of system operators is that, which PMU device(s) and signal channel(s) could provide the sufficient observability for critical oscillations of their interest, and whether further PMU deployments are necessary for monitoring critical oscillations.

In view of the above question raised by system operators, several approaches have been proposed to identify critical PMU locations for oscillation monitoring. In [5], the participation factor (PF) is applied to study the coupling relationship between oscillation modes and system state variables. However, the PF cannot provide the coupling relation-

[1]Parts of this thesis are from "Prioritization of PMU Location and Signal Selection for Monitoring Critical Power System Oscillations" by Tong Huang, Meng Wu and Le Xie, which has been submitted to IEEE Transactions on Power Systems.

ship between oscillation modes and system outputs (i.e., PMU measurements), rendering it ineffective for addressing the above problem. In [6], a geometric measure (GM) is proposed for quantifying the observability of a particular oscillation mode in system outputs. The GM is further applied to PMU placement problems for maximizing observability of modes of interest [7] and selecting control loop for wide-area controllers (WAC) [8]. In all the above applications, the objective of GM is to identify effective system outputs for improving the controller designs. However, no evidence suggests that a signal with high GM in terms of certain oscillation mode is suitable for observing this mode via the screen in front of the system operators. For candidate signals suitable for observing certain oscillation mode, a peak right at frequency of the studied mode should appear distinctly in the power spectrum density (PSD) diagram of these signals, rather than being overwhelmed by the other frequency components (modes).

In order to identify the aforementioned candidate signals, several relevant approaches have been proposed for the application of power system ambient modal estimation (AME) initially introduced in [9], [10]. In [11], factors to quantify the steepness and distinctness of the modes' spectrum are defined to select signals for AME. However, these factors are based on existing PMUs. Hence no suggestion on the further deployment of PMUs is offered, if some modes of interest cannot be observed using existing PMUs. Reference [12] introduces the modal power contribution (MPC) as a potential indicator to select signals for AME. However, the process to obtain MPC has not been given so far. In [13], based on the identified system models, the candidate signals for estimating critical modes are ranked according to the variance of the estimated damping ratios. However, the system identification techniques has some drawbacks, such as numerical artifacts [4] and order-selection problems, calling for the supplementary remedies based on the known off-line models. Besides, the purpose of [11], [12] and [13] is to select signals for estimating the critical modes, instead of directly identifying the measurements which provides sufficient observability for modes of interest, even though these two problems share a literal similarity.

In this thesis, a robust indicator, mode in output proportion factor (MOPF), is introduced for identifying critical PMU locations and signal channels, in order to better monitor power system oscillations with specific oscillation modes. Given a mode calculated from the off-line model, measurements suitable for observing it can be pinpointed. Based on the proposed MOPF, a two-layer algorithm is presented for the following purposes: 1) it identifies existing PMU devices and signal channels, which provides the best observability for critical oscillation modes; 2) it suggests the optimal locations for further PMU deployments, in order to enhance the observability for critical oscillation modes.

The rest of the thesis is organized as follows. Section 2 provides analytical decomposition of the PMU measurements into various modes; Section 3 presents newly-introduced factor MOPF and the two-layer algorithm; Section 4 validates the performance of the proposed algorithm via simulation studies; Section 5 summarizes this paper.

2. DECOMPOSITION OF PMU MEASUREMENTS INTO VARIOUS MODES

The power system small-signal dynamics around a certain operating condition can be described using the following linearized differential and algebraic equations (DAEs):

$$\dot{\boldsymbol{x}} = A\boldsymbol{x} + B\boldsymbol{u} \tag{2.1a}$$

$$\boldsymbol{y} = C\boldsymbol{x} \tag{2.1b}$$

where $\boldsymbol{x} \in \mathbb{R}^n$ is the internal state vector, representing the state deviation from the steady state of the system; $\boldsymbol{y} \in \mathbb{R}^m$ and $\boldsymbol{u} \in \mathbb{R}^d$ include m potential measurements and d inputs, respectively. $n \times n$ matrix A results from the linearizion of corresponding non-linear system around the equilibrium point. Let $\left(\lambda_1, \lambda_2, \ldots, \lambda_n\right)$, $\left(\boldsymbol{r}_1, \boldsymbol{r}_2, \ldots, \boldsymbol{r}_i, \ldots, \boldsymbol{r}_n\right)$ and $\left(\boldsymbol{l}_1^T, \boldsymbol{l}_2^T, \ldots, \boldsymbol{l}_i^T, \ldots, \boldsymbol{l}_n^T\right)^T$ denote matrix A's n distinct eigenvalues, n right eigenvectors and n left eigenvectors, respectively, where column vector $\boldsymbol{r}_i \in \mathbb{C}^n$ and row vector $\boldsymbol{l}_i \in \mathbb{C}^n$ are right and left eigenvector associating with λ_i, respectively. Each state variable is typically coupled with others in the state vector $\boldsymbol{x}$ because of the non-diagonal matrix A. Then modal decomposition is conducted to decouple all state variables. Finally, the decoupled representation of (2.1) is as follows

$$\dot{\boldsymbol{z}} = \Lambda\boldsymbol{z} + M^{-1}B\boldsymbol{u} \tag{2.2a}$$

$$\boldsymbol{y} = CM\boldsymbol{z} \tag{2.2b}$$

where $\boldsymbol{z} = \left[z_1, z_2, \ldots, z_i, \ldots, z_n\right]^T$ and z_i is ith mode associating with eigenvalue λ_i; modal matrix $M = \left[\boldsymbol{r}_1, \boldsymbol{r}_2, \ldots, \boldsymbol{r}_i, \ldots, \boldsymbol{r}_n\right]$, describing the mapping from vector $\boldsymbol{z}$ to state vector $\boldsymbol{x}$; $\Lambda = M^{-1}AM = \text{diag}\left(\lambda_1, \lambda_2, \dots, \lambda_n\right)$. M^{-1} can be denoted as

$$M^{-1} = \left[\boldsymbol{l}_1^T, \boldsymbol{l}_2^T, \dots, \boldsymbol{l}_i^T, \dots, \boldsymbol{l}_n^T\right]^T, \tag{2.3}$$

and $\boldsymbol{u}$ is $\left[u_1, u_2, \cdots, u_q, \cdots, u_d\right]^T$.

Power systems are exposed to various kinds of small disturbances, e.g. load fluctuation, and sudden small change of generator voltage reference or mechanical power. In order to obtain a time-domain expression of the mode $\boldsymbol{z}$ under the above above disturbances, each element in $\boldsymbol{u}$, say u_q, can be modeled as a step function as follows

$$u_q(t) = \begin{cases} u_q^0 & t \geq 0, \\ 0 & t < 0, \end{cases} \tag{2.4}$$

where u_q^0 is a stochastic value uniformly distributed within certain small range. At $t = 0$, $\boldsymbol{u}(0) = [u_1^0, u_2^0, \dots u_q^0, \dots u_d^0]^T$ and u_q^0 is uniformly distributed within a range of $[a, b]$, i.e.

$$u_q^0 \sim \mathcal{U}(a, b), \quad q \in \{1, 2, \cdots, d\}, \tag{2.5}$$

where $[a, b]$ are chosen such that the system can be represented by linearized model. Since all the elements in $\boldsymbol{u}$ are typically scaled to be in the per-unit from, in this paper, $[a, b]$ represents a range close to zero.

Under above assumption, the kth potential measurement in $\boldsymbol{y}$ is expressed as

$$y_k = \sum_{i=1}^{n} \left[\boldsymbol{c}_k \boldsymbol{r}_i \left(\boldsymbol{l}_i \boldsymbol{x}_0 + \frac{\boldsymbol{l}_i B \boldsymbol{u}_0}{\lambda_i}\right) e^{\lambda_i t}\right] - \sum_{i=1}^{n} \left[\boldsymbol{c}_k \boldsymbol{r}_i \frac{\boldsymbol{l}_i B \boldsymbol{u}_0}{\lambda_i}\right] \tag{2.6}$$

where $\boldsymbol{c}_k$ is the kth row of C matrix. Equation (2.6) shows that one particular measurement can be represented as the summation of the exponential terms and the constant terms under a given disturbance. Let

$$d_{ki} = \boldsymbol{c}_k \boldsymbol{r}_i \left(\boldsymbol{l}_i \boldsymbol{x}_0 + \boldsymbol{l}_i B \boldsymbol{u}_0 / \lambda_i \right) \tag{2.7}$$

. For the exponential terms associating with a pair of complex eigenvalue $\lambda_i = \alpha_i \pm j\beta_i$, their summation m_{ki} is

$$\begin{aligned} m_{ki} &= d_{ki} e^{(\alpha_i + j\beta_i)t} + \bar{d_{ki}} e^{(\alpha_i - j\beta_i)t} \\ &= 2 \left| \boldsymbol{c}_k \boldsymbol{r}_i \left(\boldsymbol{l}_i \boldsymbol{x}_0 + \frac{\boldsymbol{l}_i B \boldsymbol{u}_0}{\lambda_i} \right) \right| e^{\alpha_i t} \cos(\beta_i t + \phi_i) \end{aligned} \tag{2.8}$$

where

$$\phi_i = \tan^{-1} \frac{\mathrm{Im}\left(\boldsymbol{c}_k \boldsymbol{r}_i \left(\boldsymbol{l}_i \boldsymbol{x}_0 + \sum_{q=1}^{d} \frac{\boldsymbol{l}_i \boldsymbol{b}_q u_q^0}{\lambda_i} \right) \right)}{\mathrm{Re}\left(\boldsymbol{c}_k \boldsymbol{r}_i \left(\boldsymbol{l}_i \boldsymbol{x}_0 + \sum_{q=1}^{d} \frac{\boldsymbol{l}_i \boldsymbol{b}_q u_q^0}{\lambda_i} \right) \right)}$$

and $\bar{(\cdot)}$ is the conjugate operator.

Now we define three concepts mentioned frequently in this paper. First, as we can see in (2.8), the summation of modes $z_i(t)$ and its conjugate $\bar{z}_i$ contributes to a sinusoidal term, which represents one of the frequency components in the oscillation waveform. In order to distinguish mode definition in (2.2), we define *complex mode* m_{ki} as the summation of modes associating with a pair of conjugate eigenvalues, i.e. λ_i and $\bar{\lambda}_i$. Second, the damping ratio $\xi_i = |\alpha_i| / \sqrt{\alpha_i^2 + \beta_i^2}$ and frequency β_i manifest themselves in (2.8), so we define that the complex mode $\hat{m}_{ki}$ is the *mode of interest* if the corresponding damping ratio $\hat{\xi}_i$ is less than the user-defined threshold ϵ, and frequency $\hat{\beta}_i$ falls into a certain range. Threshold ϵ typically ranges from 0.05 to 0.1, representing poorly-damped (complex) modes. Besides, various range of frequencies can be chosen for different purposes, e.g. it can be chosen to be from 0.628 rad/s to 6.28 rad/s (0.1 Hz to 1 Hz) for observing inter-area oscillations. Third, for the sake of convenience, we define

$$\psi_{ki} = 2 \left| \boldsymbol{c}_k \boldsymbol{r}_i \left(\boldsymbol{l}_i \boldsymbol{x}_0 + \frac{\boldsymbol{l}_i B \boldsymbol{u}_0}{\lambda_i} \right) \right| \tag{2.9}$$

as the *initial amplitude* of the complex mode i in the potential measurement k, representing the amplitude of the complex mode i at $t = 0$. Built upon the aforementioned definitions, Equation (2.6) can be interpreted as a summation of complex modes, exponential terms with real eigenvalues and constant, which is

$$y_k(t) = \sum_{i \in \mathcal{M}} \psi_{ki} e^{\alpha_i} \cos(\beta_i t + \phi_i) + \sum_{i \in \mathcal{N}} d_{ki} e^{\lambda t} - \sum_{i=1}^{n} \frac{\boldsymbol{c}_k \boldsymbol{r}_i \boldsymbol{l}_i B \boldsymbol{u}_0}{\lambda_i} \tag{2.10}$$

where

$$\mathcal{M} = \{ i \in \mathbb{Z} \mid \operatorname{Im} \lambda_i > 0 \}, \quad \mathcal{N} = \{ i \in \mathbb{Z} \mid \operatorname{Im} \lambda_i = 0 \} \tag{2.11}$$

Built upon the above notation, the set of indices of modes of interest $\hat{\mathcal{M}}$ can also be expressed as a subset of $\mathcal{M}$, which is

$$\hat{\mathcal{M}} = \left\{ i \in \mathcal{M} \mid \frac{\operatorname{Re}(\lambda_i)}{|\lambda_i|} \leq \epsilon, \quad \operatorname{Im}(\lambda_i) \in [\omega_l, \omega_h] \right\} \tag{2.12}$$

where values ϵ, ω_l and ω_h can be chosen as suggested above by users. Besides, the more detail deviation is offered in Appendix A.

Equation (2.10) decomposes kth potential measurement from the theoretical perspective and connect meter-reading waveform $y_k(t)$ with complex modes. Although (2.10) indicates the potential measurement y_k incorporates components of all complex modes, not all modes can manifest themselves in y_k due to the eigen-structure of the system as well as the uncertainty of initial condition $\boldsymbol{x}_0$ and external disturbance $\boldsymbol{u}_0$. In fact, it is well accepted that each measurement has several dominant modes [3], [4]. Therefore, a potential measurement is said to be suitable for observing a given complex mode if the complex mode can manifest itself as a dominant mode in that measurement.

The physical meaning of dominant modes can be illustrated in two ways. In the context of Equation (2.10), a dominant complex mode intuitively means its initial amplitude should be relatively large compared to those of the other complex modes with similar damping ratio . From perspective of frequency domain analysis, height of the corresponding peak in the PSD of the signal can be viewed as an equivalent indicator to suggest the dominant complex modes, since there should be a distinct peak right at the frequency of the complex mode if such frequency component contributes significantly to the total energy of the signal. Therefore, a potential measurement suitable for observing a complex mode m_i with frequency f_i should have a PSD with a distinct peak right at f_i, once m_i is excited. The above discussions suggest that the initial amplitude $\psi_{k,i}$ indicates the height of the corresponding peak in the PSD of measurement y_k and, therefore, serve as an indicator to select dominant modes in a given measurement and to construct the mapping from modes of interest to measurements.

However, the initial amplitude ψ_{ki} of a complex mode in a measurement is not sufficient for determining potential measurements suitable for oscillation monitoring, since it depends on uncertain disturbances and initial conditions, compromising the consistency of result of the dominant-mode selection. Hence, we need to introduce an index which is robust under various kinds of small disturbance in a statistical sense. Besides, such index should be able to describe the relative magnitude of the initial amplitude of each complex mode and determine dominant modes in a given measurement.

3. PROPOSED INDICATOR AND ALGORITHM FOR OBSERVING MODES OF INTEREST

In this section, mode in output proportion factor (MOPF) is proposed for quantifying the significance of a certain mode in a potential measurement. Then, the comparison between the proposed MOPF and several existing indices is presented, in order to demonstrate the advantage of the MOPF. Finally, a two-layer algorithm is introduced for selecting existing PMUs and suggesting future PMU deployments to enhance the oscillation monitoring.

3.1 Mode in Output Proportion Factor (MOPF)

The MOPF of the ith complex mode within the kth measurement is defined as follows:

$$p_{ki} = E\left(\frac{\psi_{ki}}{\sum\limits_{v\in\mathcal{M}}\psi_{vk}}\right) = E\left(\frac{2\left|\boldsymbol{c}_k\boldsymbol{r}_i\left(\boldsymbol{l}_i\boldsymbol{x}_0 + \frac{\boldsymbol{l}_i B\boldsymbol{u}_0}{\lambda_i}\right)\right|}{\sum\limits_{v\in\mathcal{M}}\left|\boldsymbol{c}_k\boldsymbol{r}_v\left(\boldsymbol{l}_v\boldsymbol{x}_0 + \frac{\boldsymbol{l}_v B\boldsymbol{u}_0}{\lambda_v}\right)\right|}\right) \tag{3.1}$$

where $E(\cdot)$ is expectation operator. Equation (3.1) is explained as follows. First, the fraction term describes the relative initial amplitude ψ_i of the complex mode i in a given measurements, compared with the rest of modes in y_k. Second, such relative initial amplitude is a stochastic variable as mentioned before, so an expectation operation is conducted in order to obtain an average initial amplitude in the potential measurements based on the stochastic disturbance, rather than those due to a fixed disturbance. Third, a high value of p_{ki} suggests relatively high “proportion” of complex mode m_{ki} within given measurement y_k. If the complex mode m_{ki} happens to be of interest, the potential measurement y_k would be suitable for observing the poorly damped oscillations corresponding to m_{ki}, and distinct peak can be expected right at the frequency corresponding to m_{ki}. The MOPF defined by Equation (3.1) satisfies the two requirements presented at the end of section 2.

Recall $\boldsymbol{x}$ in (2.1) represents the state deviation from the steady state of the system, then $\boldsymbol{x}$ is a zero vector in the steady state. Besides, the disturbance is typically injected into the system through the input vector $\boldsymbol{u}$ rather than the direct perturbation of the internal state variables $\boldsymbol{x}$. Then the initial condition is assumed to be a zero vector. Therefore, Equation (3.1) reduces to

$$p_{ki} = E\left(\frac{2\left|\boldsymbol{c}_k\boldsymbol{r}_i\boldsymbol{l}_i B\boldsymbol{u}_0\lambda_i^{-1}\right|}{\sum\limits_{v\in\mathcal{M}}\left|\boldsymbol{c}_k\boldsymbol{r}_v\boldsymbol{l}_v B\boldsymbol{u}_0\lambda_v^{-1}\right|}\right), \quad i \in \mathcal{M} \tag{3.2}$$

and (2.9) reduces to

$$\psi_{ki} = 2\left|\boldsymbol{c}_k\boldsymbol{r}_i\boldsymbol{l}_i B\boldsymbol{u}_0\lambda_i^{-1}\right|, \quad i \in \mathcal{M} \tag{3.3}$$

The value of Equation (3.2) can be calculated from Monte Carlo simulation. Before presenting the detailed algorithm, the following key variables are introduced. For system (2.1) with n' complex modes and m potential measurements, there should be $m \times n'$ initial amplitude ψ and $m \times n'$ MOPFs, which can be organized in the matrix form, i.e. the *MOPF matrix*

$$P = \left[\hat{p}_{ki}\right], \tag{3.4}$$

and the *initial amplitude matrix*

$$\Psi = \left[\hat{\psi}_{ki}\right], \tag{3.5}$$

where

$$\hat{p}_{ki} = \begin{cases} p_{ki} & i \in \mathcal{M} \\ 0 & i \notin \mathcal{M} \end{cases}, \quad \hat{\psi}_{ki} = \begin{cases} \psi_{ki} & i \in \mathcal{M} \\ 0 & i \notin \mathcal{M} \end{cases} \tag{3.6}$$

In the matrix P and Ψ, the kth row corresponds to the kth potential measurement and the ith column corresponds to the ith complex mode. Finally, the algorithm for computing MOPF matrix P runs as follows:

Algorithm 1 Computing MOPF matrix

Specify simulation times τ.
Calculate Λ, M, M^{-1} based on A matrix in (2.1).
Find set $\mathcal{M}$ based on (2.11).
$\Delta \leftarrow \mathbf{0}_{m,n'}$.
for $\omega = 1$ **to** τ **do**
    Generate a set of uniformly distributed random values showing as (2.5) and set it as $\boldsymbol{u}_0$.
    Calculate each element $\hat{\psi}_{ki}$ in Ψ by (3.3) and (3.6).
    Obtain normalized matrix $\hat{\Psi} = [\hat{\psi}_{ki}]$ by

$$\hat{\psi}_{ki} = \frac{\psi_{ki}}{\sum\limits_{v \in \mathcal{M}} \psi_{kv}}$$

end for
Obtain the MOPF matrix by $P = \tau^{-1}\Delta$.

3.2 Comparison with Existing Concepts

The other two candidate indices relevant to our problem are the mode in output participation factor [14] and the geometric measure [6]. In this section, we conduct conceptual comparison between MOPF and these two existing indices.

The modes in output participation factor is built upon mode in state participation factor introduced in [15] and is defined as follows

$$p_{ki} := E\left\{\frac{\boldsymbol{l}_i \boldsymbol{x}_0 \boldsymbol{c}_k \boldsymbol{r}_i + \bar{\boldsymbol{l}}_i \boldsymbol{x}_0 \boldsymbol{c}_k \bar{\boldsymbol{r}}_i}{y_k(0)}\right\}, \tag{3.7}$$

it measures the participation of ith complex mode in the kth potential measurement. The process of defining the MOPF in (3.1) and the factor in (3.7) share similarity in terms of dealing with uncertainty in the system. Both concepts assumes that the evolution of complex modes does not only depend on the system inherent property, i.e. the eigenstructure, but are also determined by the disturbance uncertainties. Hence, both concepts consider the effect of disturbance uncertainties.

However, the physical meanings of these two factors are difference. In order to explore the physical meanings of the two factors, assume that the disturbance is injected into the system through the internal state variable $\boldsymbol{x}_0$, that is $\boldsymbol{u}_0 = \mathbf{0}$, then the complex mode m_{ki} in (2.8) reduces into

$$m_{ki} = 2\left|\boldsymbol{l}_i\boldsymbol{x}_0\boldsymbol{c}_k\boldsymbol{r}_i\right| e^{\alpha_i t}\cos(\beta_i t + \phi_i) \tag{3.8}$$

where

$$\phi_i = \tan^{-1}\frac{\mathrm{Im}(\boldsymbol{l}_i\boldsymbol{x}_0\boldsymbol{c}_k\boldsymbol{r}_i)}{\mathrm{Re}(\boldsymbol{l}_i\boldsymbol{x}_0\boldsymbol{c}_k\boldsymbol{r}_i)}.$$

At $t = 0$, $m_{ki}(0) = \mathrm{Re}(\boldsymbol{l}_i\boldsymbol{x}_0\boldsymbol{c}_k\boldsymbol{r}_i)$, which exactly is numerator of (3.7). Therefore, the mode in output participation factor describes the percentage of the complex mode i in the initial value of kth output y_{k0}. If a potential measurement y_k can be viewed as the superposition of complex modes, decaying exponential terms and a constant as in (2.10), the mode in output participation factor in (3.7) can be employed to suggest the relative magnitudes of complex modes, rather than their initial amplitudes. However, the initial amplitude of the complex mode serves as a direct indicator of the height of the corresponding peak in the PSD, whereas the factor in (3.7) only offers a lower bound of the initial amplitude. Therefore, there is no direct connection between the mode in output participation factor and this renders Equation (3.7) improper to serve as indicator for identifying critical PMU signals to monitor the oscillation modes of interest.

Geometric measure (GM) overcomes the limitation that Popov-Belevitch-Hautus (PBH) test only can offer a yes-or-no answer, and is designed to measure the modal controllability and observability [6]. The GM of modal observability of mode i for system (2.1) in measurement k is defined as follows [6]

$$g_{k,i} = \cos\left[\theta(\boldsymbol{c}_k, \boldsymbol{r}_i^T)\right] = \frac{\left|\boldsymbol{c}_{\boldsymbol{k}}\boldsymbol{r}_i^T\right|}{\left\|\boldsymbol{c}_{\boldsymbol{k}}\right\|\left\|\boldsymbol{r}_i^T\right\|} \tag{3.9}$$

where $|\cdot|$ is the magnitude of a complex value and $\|\cdot\|$ is 2-norm of a vector. Though its physical meaning can be explained from energy point of view [6], in the context of capturing modes of interest directly by decomposing raw measurements, such an explanation becomes obscured owning to ignorance of initial condition in (2.6). Further comparison will also be presented in part 4 via simulation.

3.3 Threshold Selection for Dominant Complex Mode in Given Measurement

In this section, we present a quantitative threshold in terms of initial amplitude ψ_{ki} to determine the suitable signals for observing a given modes of interest. The k-th candidate signal is said to be suitable for observing the i-th complex mode if its MOPF p_{ki} satisfies $p_{ki} \geq \gamma \sup_{v\in[1,2,\cdots,m]} p_{vi}$, where γ is a user-defined parameter and is empirically set to be 0.75 in this paper. Meanwhile, we define

$$\mathcal{K}_i = \left\{ i \in \mathbb{Z} \mid p_{ki} \geq \gamma \sup_{v\in\mathcal{M}} p_{kv}, \quad i \in \mathcal{M} \right\}. \tag{3.10}$$

$\mathcal{K}_i$ in Equation (3.10) can be employed to find the indices of the possible measurements suitable for observing a given complex mode i.

3.4 Hierarchical Scheme for Optimal PMU Placement and Signal Selection

Some PMUs have already been deployed in the system based on either engineering intuition or requirements of standards, so the classical PMU-placement problem can be further broken into the following sub-problems: 1) identify the existing PMU signals that are most appropriate for observing a particular mode of interest; 2) identify the best locations for installing new PMUs, which could observe a particular mode that is unobservable using existing PMUs.

The first layer of the algorithm checks whether the further deployment of PMUs is needed and identify the best PMU signals for observing the modes of interest. Typically, one PMU has multiple channels, which allows us to observe all kinds of measurements relative to the bus where this PMU is installed. Suppose the set $\mathcal{B}$ collects the indices of the buses equipped with PMUs and each element in the set $\mathcal{G}_k$ represents the indice of PMU channel installed at Bus k, then the first-layer algorithm is presented as follows:

Algorithm 2 Layer 1: the existing signals selection

$H \leftarrow \mathbf{0}_{m,n}$; find $\hat{\mathcal{M}}$ by (2.12); $\hat{\mathcal{M}}_{\text{observed}} \leftarrow \varnothing$.
for $i \in \hat{\mathcal{M}}$ **do**
  Find $\mathcal{K}_i$ by (3.10).
  $h_{vi} \leftarrow 1, \quad \forall v \in \mathcal{K}_i$.
  for $k \in \mathcal{B}$ **do**
    if $\mathcal{G}_k \cap \mathcal{K}_i \neq \varnothing$ **then**
      $\hat{\mathcal{M}}_{\text{observed}} \leftarrow \hat{\mathcal{M}}_{\text{observed}} \cup \{i\}$.
      Mode of interest i could be observed by the PMU installed at bus k via measurement $\arg\max_{v \in \mathcal{G}_k \cap \mathcal{K}_i} p_{vi}$.
    end if
  end for
end for
if $\hat{\mathcal{M}} - \hat{\mathcal{M}}_{\text{observed}} = \varnothing$ **then**
  All modes of interest can be reliably captured by existing PMUs.
else
  Further deployment of PMU is needed.
end if

The set $\hat{\mathcal{M}}_{\text{observed}}$ stores the indices of complex modes which cannot be reliably observed from existing PMUs, so further deployment should be conducted for observing the complex modes in $\hat{\mathcal{M}}_{\text{observed}}$. In order to limit or minimize the number of further deployed PMUs, the selected buses for installing PMUs should allow us to observe as many modes of interest as possible using PMU signals from various channels.

For the sake of convenience, the following definitions are presented. Suppose the system represented by (2.1) has m' buses, each bus includes several potential measurements in $\boldsymbol{y}$. Besides, $m' \times n$ matrix $\hat{H} = [\hat{h}_{kv}]$ is denoted by $[\hat{\boldsymbol{h}}_1^T, \hat{\boldsymbol{h}}_2^T, \cdots, \hat{\boldsymbol{h}}_k^T, \cdots, \hat{\boldsymbol{h}}_{m'}^T]^T$ where $\hat{\boldsymbol{h}}_k \in \mathbb{R}^n$ is a row vector. Meanwhile, $\hat{H}$ can also be denoted by $[\hat{\boldsymbol{h}'}_1, \hat{\boldsymbol{h}'}_2, \cdots, \hat{\boldsymbol{h}'}_i, \cdots, \hat{\boldsymbol{h}'}_n]$, where $\hat{\boldsymbol{h}'} \in \mathbb{R}^{m'}$ is a column vector. Similarly, $m \times n$ matrix H can be denoted by $[\boldsymbol{h}_1^T, \boldsymbol{h}_2^T, \cdots, \boldsymbol{h}_v^T, \cdots, \boldsymbol{h}_{m'}^T]^T$.

Then the second layer algorithm is introduced to identify the optimal locations for installing new PMUs, in order to observe the modes of interest that are unobservable using existing PMUs.

Algorithm 3 Layer 2: further deployment of PMUs

$\hat{H} \leftarrow \mathbf{0}_{n,m'}$.
for $k = 1$ **to** m' **do**
  $\hat{\boldsymbol{h}}_k \leftarrow \sum_{v \in \mathcal{G}_k} \boldsymbol{h}_v$.
  $\hat{h}_{kv} \leftarrow 1, \quad \forall v \in \{i \in \mathbb{Z} \mid h_{ki} > 1\}$.
end for
$\hat{\mathcal{M}}_n \leftarrow \hat{\mathcal{M}} - \hat{\mathcal{M}}_{\text{observed}}$.
while $\hat{\mathcal{M}}_n \neq \varnothing$ **do**
  $\boldsymbol{s} = \sum_{i \in \hat{\mathcal{M}}_n} \boldsymbol{h'}_i$, denoting by $[s_1, s_2, \cdots, s_k, \cdots, s_{m'}]^T$
  PMU should be installed in $\hat{k}$-th bus, where

$$\hat{k} = \arg\max_k s_k.$$

  Find $\mathcal{I}_{\hat{k}}$ by $\mathcal{I}_{\hat{k}} = \{i \in \mathbb{Z} \mid h_{\hat{k}i} = 1\}$.
  for $k \in \mathcal{G}_{\hat{k}}$ **do**
    Find $\mathcal{I}_{\hat{k}}$ by $\mathcal{I}_k = \{i \in \mathbb{Z} \mid h_{ki} = 1\}$.
    if $\mathcal{I}_k \cap \mathcal{I}_{\hat{k}} \neq \varnothing$ **then**
      Mode of interest $\mathcal{I}_k \cap \mathcal{I}_{\hat{k}}$ could be observed by the PMU installed at bus $\hat{k}$ via measurement k.
    end if
  end for
  $\hat{\mathcal{M}}_n \leftarrow \hat{\mathcal{M}}_n - \mathcal{I}_{\hat{k}}$.
end while

It is worth pointing out that the proposed two-layer algorithm also works in systems without existing PMUs. In this case, layer 1 is skipped due to $\mathcal{B} = \varnothing$.

4. CASE STUDIES

The performance of newly-introduced indicator MOPF and the two-layer algorithm is validated in the modified benchmark 68-bus system (Fig.4.1 [16]) and the Northeastern Power Council (NPCC) 140-bus system. The raw parameters for the both systems are available in the Power System Toolbox (PST) [17]. In the both cases, the threshold ϵ, f_l and f_h in (2.12) are set to be 5%, 0.1Hz and 2Hz, respectively. Besides, stochastic disturbances in both test systems are modeled as random changes on voltage references of voltage regulators $\boldsymbol{V}_{ref}$, mechanical power injections $\boldsymbol{P}_m$ and real and reactive power of loads $\boldsymbol{P}_l$ and $\boldsymbol{Q}_l$. The above three components constitutes the vector $\boldsymbol{u}_0$ and each element u_q^0 is uniformly distributed within $[-0.1, 0.1]$.

4.1 Results of Two-layer Algorithm and Its Validation for the 68-bus System

4.1.1 68-Bus System Description

For the 68-bus system, three main modifications based on raw parameters are made to the raw parameters. First, in order to obtain poorly-damped complex modes, the gain-washout time constant of the power system stabilizers (PSS) at generator 9 is set to 200, and the PSSs at the rest of generators are disabled. Second, load modulations of real and reactive power are added to simulate the stochastic load fluctuation. Third, the load and generation levels are set to be 65% of the original level. Then, all the modal parameters of modes of interest listed in Table 4.1 can be calculated based on matrix A, B and C in (2.1).

In this test case, several existing PMUs are introduced, based on the following engineering intuition: First, generators with relatively large capacity are considered as "important" generators, thus buses near those generators should be equipped with PMUs. Second, PMU deployment should spread over the whole grid, rather than focus on a limited area.

Hence, the existing PMUs are installed at Bus 2, 10, 19, 36 and 52.

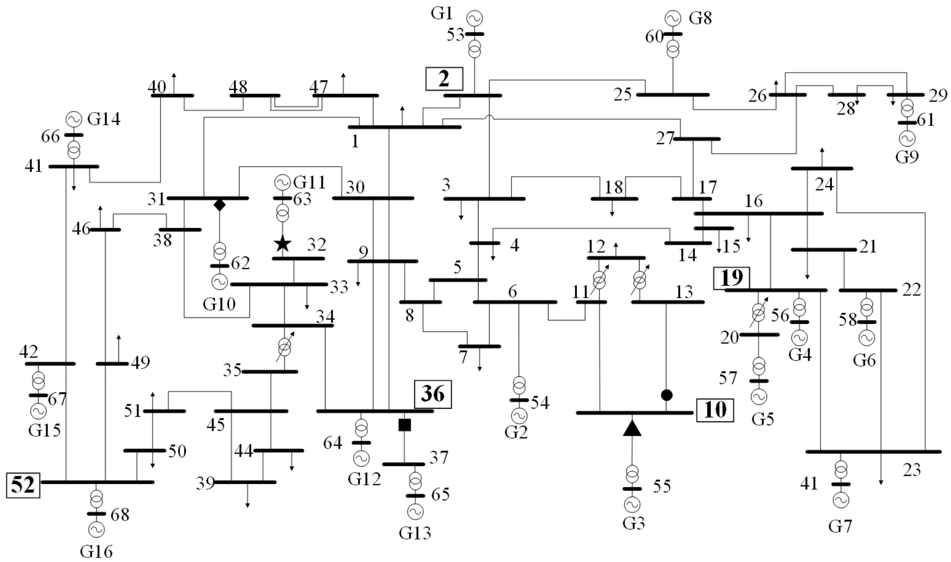

Figure 4.1: 68-bus test system: numbers of buses equipping with PMU are boxed; the geographic locations of each selected channel in Table 4.1 are marked

4.1.2 Results for the Two-layer Algorithm

Table 4.1 contains the result of each layer of the algorithm. The first-layer algorithm selects PMU channels specifically for observing complex mode 183 and 189 from existing PMUs. Since not all the modes of interest can be observed from existing PMUs, further deployment is needed. Then the second-layer algorithm identifies the suitable locations for installing new PMUs. Finally, we expect that modes of interest should manifest themselves in waveforms recorded by their corresponding channels, if those complex modes are excited.

Table 4.1: Result of Two-layer Algorithm for 68-bus System

Layer	**Selected Channel**	i	$\xi_i(\%)$	$f_i(Hz)$
1	P from Bus 10 to 13	181	4.96	1.11
	P from Bus 36 to 37	183	3.62	1.16
	P from Bus 10 to 55	189	3.98	1.27
2	P from Bus 31 to 62	193	3.06	1.30
	P from Bus 32 to 63	207	3.64	1.88

4.1.3 PSD Validation

In order to compare the performance between selected and unselected PMUs in terms of observing modes of interest, waveforms recorded by all the potential measurements under a stochastic disturbance should be obtained. To achieve this, the test system is represented by the state-space model in (2.1) with 98×1 input vector $\boldsymbol{u}(t)$ and 525×1 output vector $\boldsymbol{y}(t)$. After a 30-second simulation, the output vector $\boldsymbol{y}$ offers 525 sets of time series and each of them contains 30×60 samples, representing 60-second waveforms recorded by 525 measurement channels of PMUs with a sampling rate of 60Hz. Besides, Gaussian noise with a signal-to-noise ratio (SNR) of 45dB is added to each set of time series. Finally, frequency components of each waveform can be analyzed via Fast Fourier Transformation (FFT).

In our test case, instead of monitoring all the 525 waveforms, we only need to monitor five PMU channels for determining whether the modes of interest are excited. If a mode of interest is excited by a disturbance, this complex mode would manifest itself as a dominant complex mode in the selected PMU channel specifically selected for it. Therefore, a peak would appear right at its frequency in the PSD. Fig. 4.2 presents the PSD of waveforms recorded by selected channels under certain disturbance. These figures inform operators that all the five modes of interest are excited, due to the five peaks at frequencies of these complex modes.

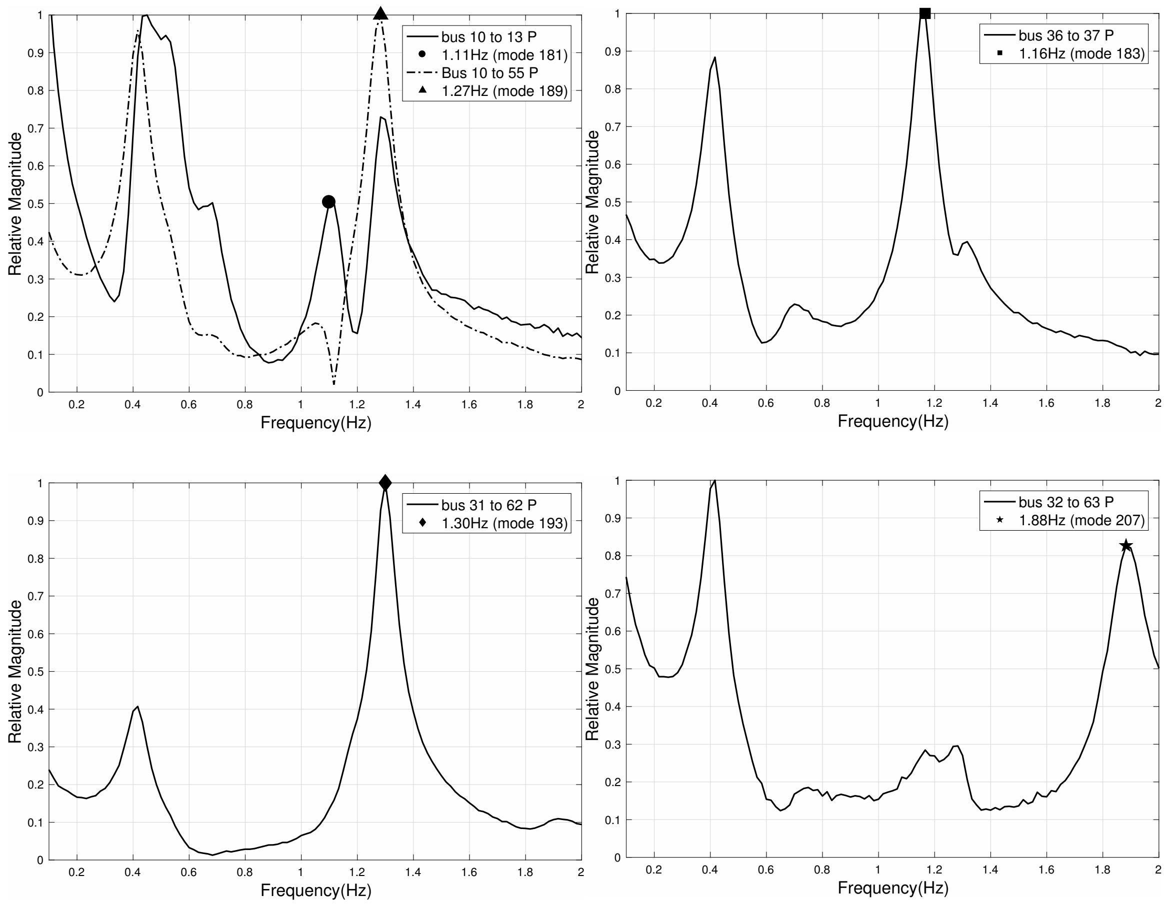

Figure 4.2: PSD of selected signals for 68-bus system in Table 4.1. The marked peaks indivate all 5 modes of interest are excited.

4.2 Results of Two-layer Algorithm and Its Validation for the NPCC 140-bus System

For the NPCC 140-bus system, load modulations of real and reactive power are added to the original system provided by PST. Then, the matrix A, B and C in (2.1) can be extracted by PST, and all the modes of interest in this case are listed in Table 4.2. Besides, based on the engineering intuition, the existing PMUs are installed at Bus 22, 54, 71, 101 and 135.

Table 4.2 presents the result of each layer of algorithm. The existing PMU at Bus 71 is selected for observing the complex mode 295, and the locations of PMUs for observing the rest of modes of interest are also suggested by the second layer algorithm. As we can observed from Table 4.2, in terms of bus selection, the second layer algorithm gives high priorities to the buses enabling us to observe multiple modes of interest. Hence, suppose there is no existing PMU, only 7 buses should be equipped with PMUs, although there are 13 modes of interest. Besides, Fig. 4.3 shows each modes of interest manifests itself in the signal selected for monitoring it.

Table 4.2: Result of Two-layer Algorithm for the NPCC 140-bus System

Bus	**Selected Channel**	i	$\xi_i(\%)$	f_i (Hz)
71	Frequency Deviation	295	4.53	0.91
8	P from Bus 8 to 9	181	1.37	0.62
	P from Bus 8 to 18	293	3.79	0.89
53	P from Bus 53 to 52	325	4.51	1.16
	P from Bus 53 to 65	371	2.53	1.64
68	Frequency deviation	375	2.41	1.68
		385	2.05	1.99
92	P from Bus 92 to 97	327	4.82	1.22
	Q from Bus 92 to 97	359	3.15	1.42
117	P from Bus 117 to 121	321	4.51	1.16
	P from Bus 117 to 119	383	2.15	1.85
118	P from Bus 118 to 123	365	2.98	1.49
		373	2.41	1.68

4.3 Convergence Test of MOPF

The MOPF is calculated via Monte Carlo simulation, so a natural question is whether the result of MOPF depends on the simulation time τ. Fig. 4.4 visualizes the variation of 5 elements in MOPF as simulation times τ changes from 50 to 10,000 times. As shown in

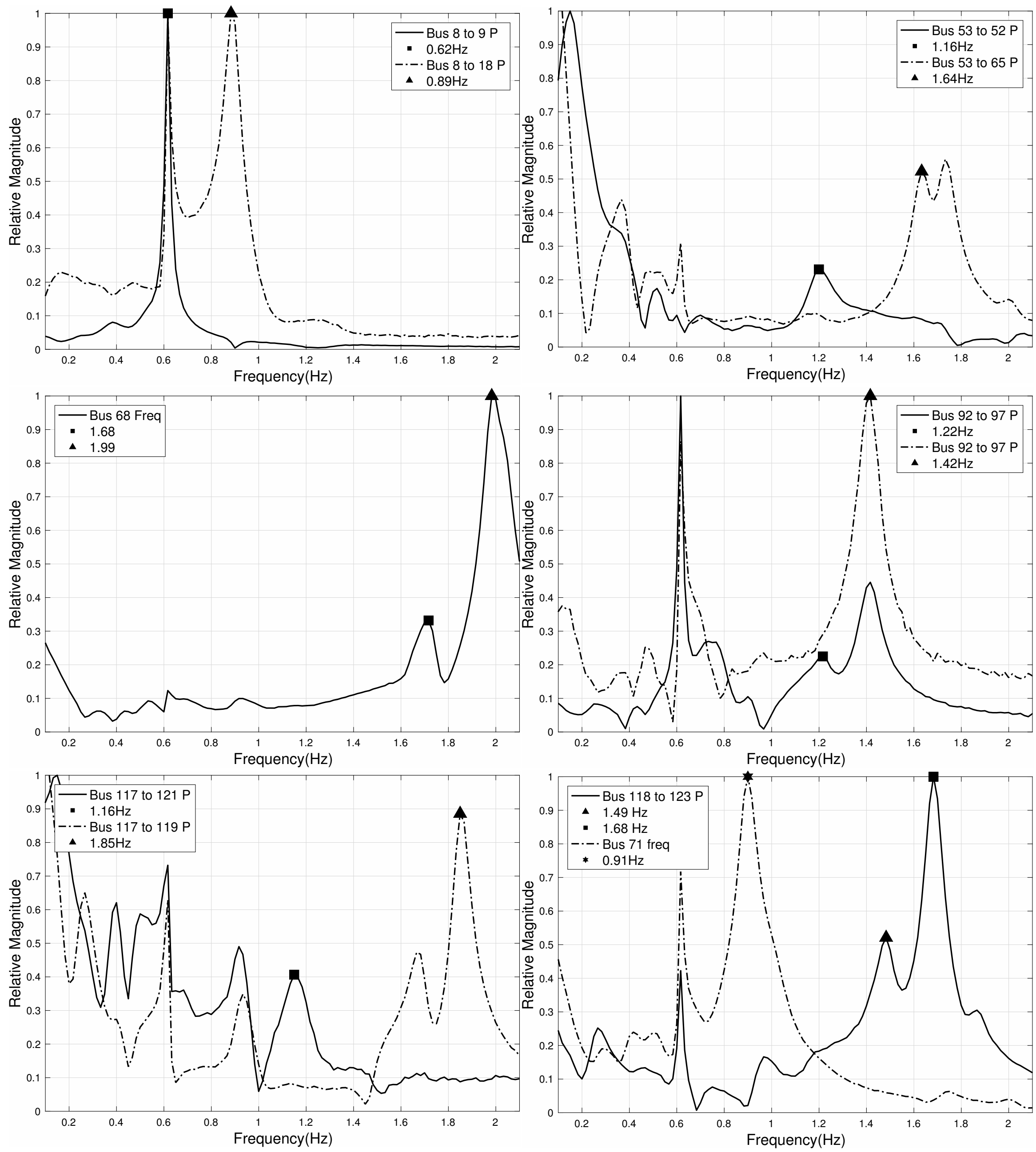

Figure 4.3: PSD of selected signals for NPCC 140-bus system in Table 4.2.

Fig. 4.4, the selected elements in the MOPF matrix tend to be bounded as simulation time τ increases.

In order to reflect the overall variation of the MOPF matrix $[p_{k,i}]$ due to the variation of the simulation time, we introduce the maximum deviation e_m^τ and average deviation e_a^τ:

$$e_m^\tau = \sup_{\substack{k\in[1,2,\cdots,m]\\ i\in\mathcal{M}}} \frac{\left|p_{k,i}^\tau - p_{k,i}^{10,000}\right|}{p_{k,i}^{10,000}} \tag{4.1}$$

and

$$e_a^\tau = \frac{1}{m\times|\mathcal{M}|}\sum_{k=1}^{m}\sum_{i\in\mathcal{M}} \frac{\left|p_{k,i}^\tau - p_{k,i}^{10,000}\right|}{p_{k,i}^{10,000}}, \tag{4.2}$$

where $p_{k,i}^\tau$ represents the element at kth row and ith column of the MOPF matrix calculated when the simulation time is τ. The decreasing trend shown in Fig. 4.5 suggests the impact of simulation time τ on the elements in MOPF matrix is limited as τ increases. Furthermore, the weak correlation between the MOPF matrix and the simulation time τ validates that the MOPF matrix can serve as a robust indicator to identify suitable PMUs for observing the modes of interest under uncertain disturbances.

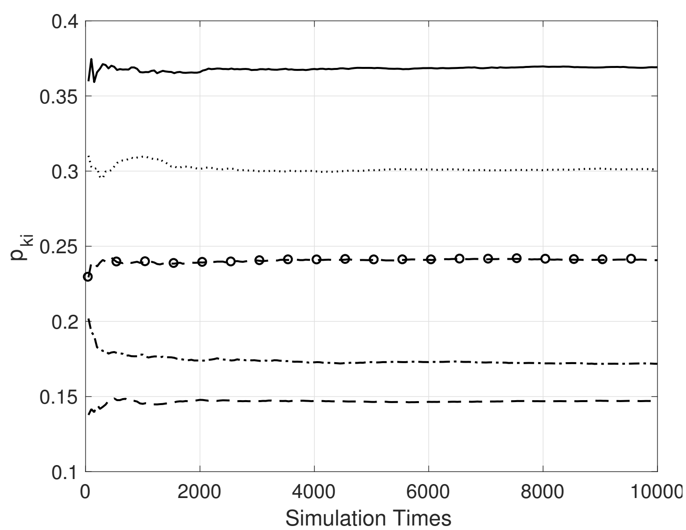

Figure 4.4: The variation of $p_{262,183}$ (solid line), $p_{201,189}$ (dash-dot line), $p_{195,181}$ (dash line), $p_{260,193}$ (dot line) and $p_{261,207}$ (dash-circle line) in MOPF matrix

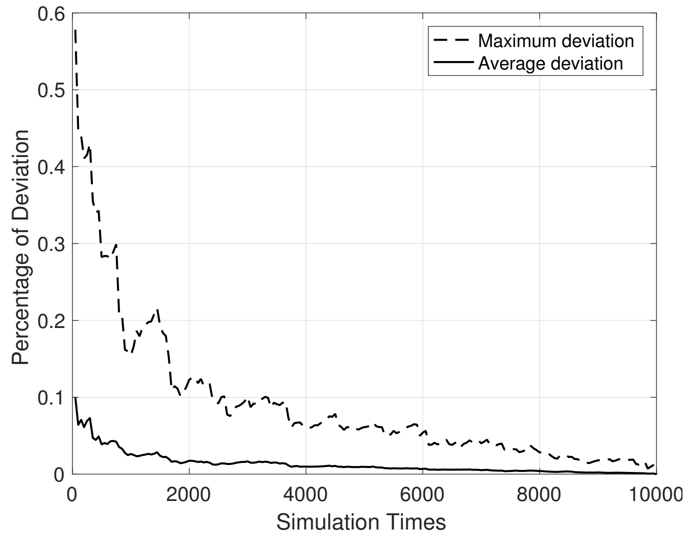

Figure 4.5: The evolution of e_a^τ (solid line) and e_m^τ (dash line).

4.4 Impact of Uncertain Disturbance on Proportion of Complex Modes in Measurements

Under certain disturbance, some unselected meters seem to be suitable for observing modes of interest. For example, under disturbance $\boldsymbol{u}_1$, the PSD of PMU installed in bus 65 of the 68-bus system (dot line in the left figure of Fig. 4.6) shows a distinct peak right at the frequency of the mode of interest, then this PMU might be also considered suitable for observing complex mode 183 besides PMU at bus 36. However, under another disturbance $\boldsymbol{u}_2$, that a distinct peak corresponding to complex mode 183 is presented in the real power waveform from Bus 36 to Bus 37, whereas no distinct peak corresponding to the complex mode 183 can be observed in the real power waveform from bus 65 to bus 37. It is shown in the right figure of Fig. 4.6, that a distinct peak corresponding to complex mode 183 is presented in the real power waveform from Bus 36 to Bus 37, whereas no distinct peak corresponding to the complex mode 183 can be observed in the real power waveform from bus 65 to bus 37. Thus, real power from bus 65 to 37 might not be suitable for observing the complex mode 183. Although the disturbance uncertainties causes the variation in the of the peak marked with square in the left figure of Fig. 4.6, it is sufficient to conclude that complex mode 183 is excited.

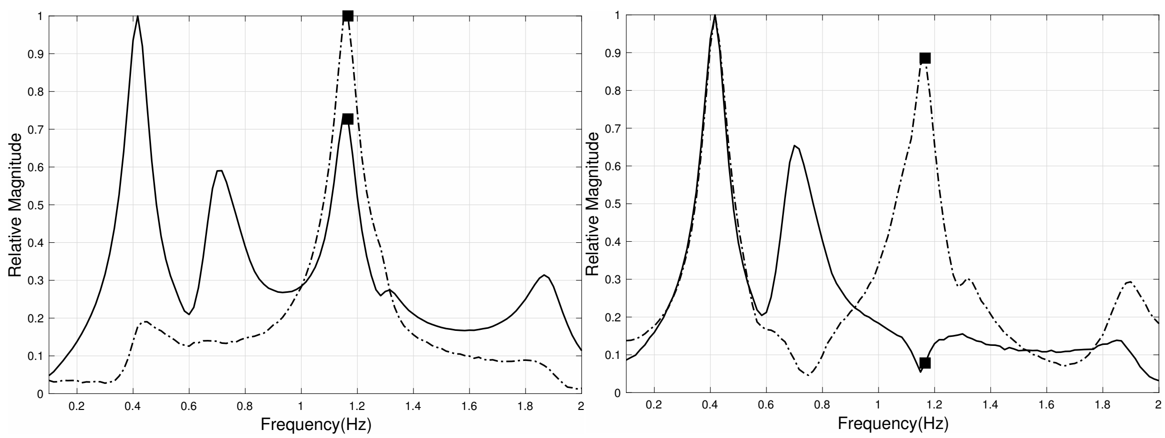

Figure 4.6: PSD of real power from bus 36 to 37 (left) and real power from bus 65 to 37 (right) under disturbance $\boldsymbol{u}_1$ (dot line) and $\boldsymbol{u}_2$ (solid line) in the 68-bus system.

Another demonstrative scenario can be synthesized from Fig. 4.6 to articulate the necessity for this research. Suppose only the channel measuring real power from bus 65 to 37 is monitored, the operators may only observe the two uninterested complex modes below 1Hz, and might not be sure whether the complex mode 183 is excited when disturbance $\boldsymbol{u}_2$ happens. Therefore, they might not take any action due to relatively high damping ratio of those two modes. However, the system is suffering from the sustained oscillation caused by complex mode 183, which may not be observed through the monitored PMU channel. However, if the PMU channel from bus 36 to bus 37 is monitored, the poorly-damped complex mode 183 could be observed by system operators.

4.5 Comparison with Geometric Measure

Now we present the performance comparison between MOPF and GM in terms of observing complex modes. To perform comparison, the MOPF $\hat{p}_{k,i}$ and GM $\hat{g}_{k,i}$ are normalized by dividing $\sup_{v \in \mathcal{M}} p_{k,v}$ and $\sup_{v \in \mathcal{M}} g_{k,v}$, respectively.

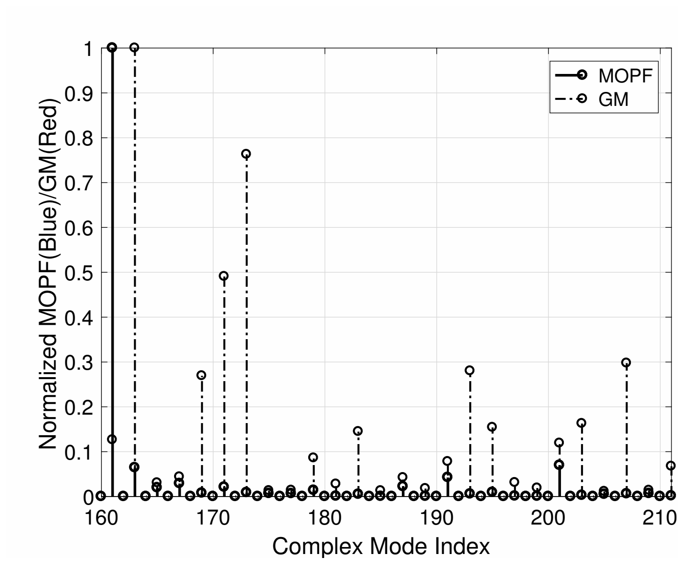

Figure 4.7: Discrepancy between MOPF (solid line) and GM (dash-dot line) of meter measuring reactive power from bus 1 to 2.

The channel measuring reactive power from bus 1 to 2 is selected for comparing the accuracy of the two indices. Fig. 4.7 is the visualization of MOPF (solid line) and GM (dash-dot line) for this channel. It shows an obvious discrepancy between MOPF and GM: MOPF indicates this meter is suitable for observing the complex mode 161 with a frequency of 0.0043Hz, whereas GM suggests this meter is suitable for observing the complex mode 163 with a frequency of 0.4162Hz. If GM is reliable, we would expect a peak around 0.4162Hz in PSD of the waveform recorded by this channel, when this complex mode is excited. However, according to the solid line in Fig. 4.8, complex the

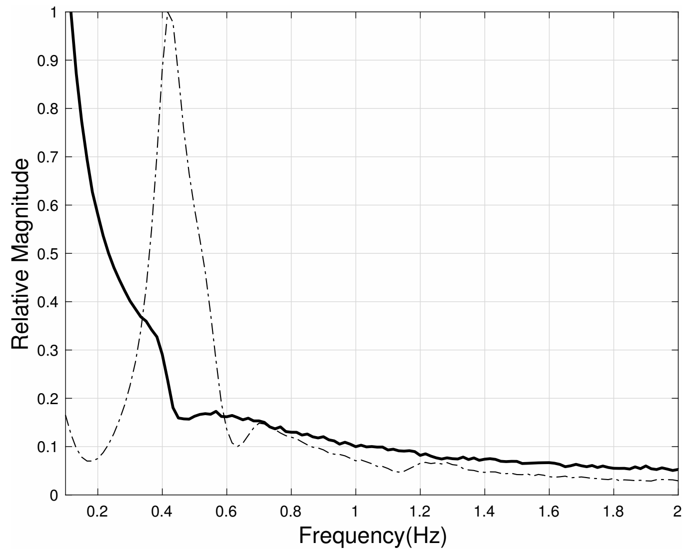

Figure 4.8: PSD of reactive power from bus 1 to 2 (solid line) and real power from bus 39 to 44 (dash-dot line).

mode 163 does not manifest itself at the aforementioned channel, while it is indeed excited due to the appearance of a peak around 0.4162Hz in the PSD of another PMU waveform (dash-dot line). Thus, GM might not be able to serve as a reliable index for identifying suitable PMU signals in order to observe the modes of interest.

4.6 Robustness Test

In this section, we explore the robustness of the proposed algorithm with respect to the load fluctuation. For a given mode of interest i, the first-layer algorithm offers a set of measurements $\mathcal{K}_i^{\mathcal{C}}$ suitable for observing the complex mode i, based on the operating conditions denoted by set $\mathcal{C}$. Since the MOPF matrix in the preceding discussion is computed based one loading condition, i.e. $\mathcal{C} = \{100\%\}$, one might expect to know the changes of the result of the first-layer algorithm, $\mathcal{K}_i^{\bar{\mathcal{C}}}$, under other loading conditions $\bar{\mathcal{C}}$, compared with $\mathcal{K}_i^{\mathcal{C}}$. In order to quantify the overlap of results under two different loading condition, define

$$r_i^{\bar{\mathcal{C}}} = \frac{\left|\mathcal{K}_i^{\mathcal{C}} \cap \mathcal{K}_i^{\bar{\mathcal{C}}}\right|}{\left|\mathcal{K}_i^{\mathcal{C}}\right|}, \tag{4.3}$$

where $\bar{\mathcal{C}} \in \{50\%, 55\%, \cdots, 150\%\}$ and each element represents the percentage of the loading condition in the original test case. Then $r_i^{\bar{\mathcal{C}}}$ can be visualized as in Fig. 4.9. It suggests that the result of the first-layer algorithm under the loading condition $\mathcal{C}$ can also be applied in the system under the rest of the loading condition $\bar{\mathcal{C}}$, for the complex modes with frequencies around 1.16 Hz, 1.27 Hz, 1.3 Hz and 1.88 Hz.

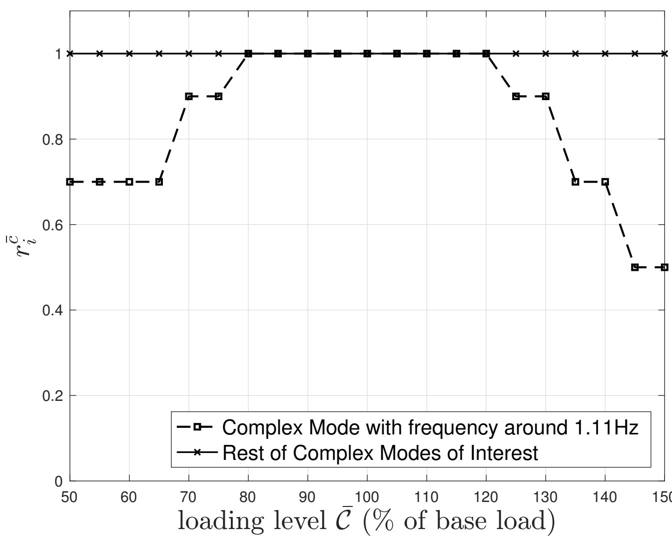

Figure 4.9: Visualization of $r_i^{\bar{\mathcal{C}}}$ for the 68-bus system.

5. CONCLUSION

This thesis introduced a robust indicator, MOPF, for identifying critical PMU locations and signal channels, in order to better monitor power system oscillations with specific oscillation modes. Based on the proposed MOPF, two-layer algorithm is presented. System operators and planners can be benefited from this algorithm in the following two ways: 1) it identifies existing PMU devices and signal channels, which provides sufficient observability for critical oscillation modes; 2) it suggests optimal locations for further PMU deployments, in order to enhance the observability for critical oscillation modes. From a research perspective, this paper points out that the distribution of modal information among all measurements depends both on the system parameters and the characteristics of the disturbance.

REFERENCES

[1] L. Xie, Y. Chen, and P. R. Kumar, "Dimensionality reduction of synchrophasor data for early event detection: Linearized analysis," *IEEE Transactions on Power Systems*, vol. 29, pp. 2784–2794, Nov 2014.

[2] J. D. L. Ree, V. Centeno, J. S. Thorp, and A. G. Phadke, "Synchronized phasor measurement applications in power systems," *IEEE Transactions on Smart Grid*, vol. 1, pp. 20–27, June 2010.

[3] J. Ning, S. A. N. Sarmadi, and V. Venkatasubramanian, "Two-level ambient oscillation modal estimation from synchrophasor measurements," *IEEE Transactions on Power Systems*, vol. 30, pp. 2913–2922, Nov 2015.

[4] D. J. Trudnowski, J. W. Pierre, N. Zhou, J. F. Hauer, and M. Parashar, "Performance of three mode-meter block-processing algorithms for automated dynamic stability assessment," *IEEE Transactions on Power Systems*, vol. 23, pp. 680–690, May 2008.

[5] I. J. Perez-arriaga, G. C. Verghese, and F. C. Schweppe, "Selective modal analysis with applications to electric power systems, part i: Heuristic introduction," *IEEE Transactions on Power Apparatus and Systems*, vol. PAS-101, pp. 3117–3125, Sept 1982.

[6] A. Hamdan and A. Elabdalla, "Geometric measures of modal controllability and observability of power system models," *Electric Power Systems Research*, vol. 15, no. 2, pp. 147 – 155, 1988.

[7] A. M. Almutairi and J. V. Milanovic, "Comparison of different methods for optimal placement of pmus," in *2009 IEEE Bucharest PowerTech*, pp. 1–6, June 2009.

[8] A. Heniche and I. Karnwa, “Control loops selection to damp inter-area oscillations of electrical networks,” *IEEE Transactions on Power Systems*, vol. 17, pp. 378–384, May 2002.

[9] J. W. Pierre, D. J. Trudnowski, and M. K. Donnelly, “Initial results in electromechanical mode identification from ambient data,” *IEEE Transactions on Power Systems*, vol. 12, pp. 1245–1251, Aug 1997.

[10] R. W. Wies, J. W. Pierre, and D. J. Trudnowski, “Use of arma block processing for estimating stationary low-frequency electromechanical modes of power systems,” *IEEE Transactions on Power Systems*, vol. 18, pp. 167–173, Feb 2003.

[11] J. Zhang, C. Wu, and Y. Han, “A power spectrum density based signal selection approach for electromechanical mode estimation,” in *2012 IEEE Power and Energy Society General Meeting*, pp. 1–7, July 2012.

[12] D. J. Vowles and M. J. Gibbard, “Illustration of an analytical method for selecting signals and locations for power system modal-estimators,” in *IEEE PES General Meeting*, pp. 1–7, July 2010.

[13] V. S. PeriÄĞ, X. Bombois, and L. Vanfretti, “Optimal signal selection for power system ambient mode estimation using a prediction error criterion,” *IEEE Transactions on Power Systems*, vol. 31, pp. 2621–2633, July 2016.

[14] L. Sheng, E. H. Abed, M. A. Hassouneh, H. Yang, and M. S. Saad, “Mode in output participation factors for linear systems,” in *Proceedings of the 2010 American Control Conference*, pp. 956–961, June 2010.

[15] W. A. Hashlamoun, M. A. Hassouneh, and E. H. Abed, “New results on modal participation factors: Revealing a previously unknown dichotomy,” *IEEE Transactions on Automatic Control*, vol. 54, pp. 1439–1449, July 2009.

[16] H. Bevrani, M. Watanabe, and Y. Mitani, *Power system monitoring and control*. John Wiley & Sons, 2014.

[17] J. H. Chow and K. W. Cheung, “A toolbox for power system dynamics and control engineering education and research,” *IEEE Transactions on Power Systems*, vol. 7, pp. 1559–1564, Nov 1992.

APPENDIX A

DERIVATION OF MODE IN OUTPUT PROPORTION IN STATISTICAL WAY

State-space representation of power system is

$$\dot{\boldsymbol{x}} = A\boldsymbol{x} + B\boldsymbol{u} \tag{A.1a}$$

$$\boldsymbol{y} = C\boldsymbol{x} \tag{A.1b}$$

where

1. $\boldsymbol{x} \in \mathbb{R}^n$ is internal state vector of system
2. $\boldsymbol{y} \in \mathbb{R}^m$ includes m potential measurements
3. $\boldsymbol{u} \in \mathbb{R}^d$
4. $n \times n$ matrix A results from linearizion of corresponding non-linear system around equilibrium point.
5. Let $\left(\lambda_1, \lambda_2, \ldots, \lambda_n\right)$, $\left(\boldsymbol{r}_1, \boldsymbol{r}_2, \ldots, \boldsymbol{r}_i, \ldots, \boldsymbol{r}_n\right)$ and $\left(\boldsymbol{l}_1^T, \boldsymbol{l}_2^T, \ldots, \boldsymbol{l}_i^T, \ldots, \boldsymbol{l}_n^T\right)^T$ denote matrix A's n distinct eigenvalues, n right eigenvectors and n left eigenvectors, respectively, where column vector $\boldsymbol{r}_i \in \mathbb{C}^n$ and row vector $\boldsymbol{l}_i \in \mathbb{C}^n$ are right and left eigenvector associating with λ_i, respectively.
6. $d \times n$ matrix B is input matrix, denoted by $\left(\boldsymbol{b}_1, \boldsymbol{b}_2, \ldots, \boldsymbol{b}_i, \ldots, \boldsymbol{b}_n\right)$
7. Real $m \times n$ matrix C represents a mapping from n state variables to m potential measurements.

Introducing transformation

$$\boldsymbol{x} = M\boldsymbol{z} \tag{A.2}$$

then decoupled representation of (A.1) follows

$$\dot{\boldsymbol{z}} = \Lambda\boldsymbol{z} + M^{-1}B\boldsymbol{u} \tag{A.3a}$$

$$\boldsymbol{y} = CM\boldsymbol{z} \tag{A.3b}$$

where

1. $\Lambda = M^{-1}AM = diag\left(\lambda_1, \lambda_2, \ldots, \lambda_n\right)$.
2. M^{-1} can be denoted as $\left[\boldsymbol{l}_1^T, \boldsymbol{l}_2^T, \ldots, \boldsymbol{l}_i^T, \ldots, \boldsymbol{l}_n^T\right]^T$.
3. Modal matrix $M = \left[\boldsymbol{r}_1, \boldsymbol{r}_2, \ldots, \boldsymbol{r}_i, \ldots, \boldsymbol{r}_n\right]$

$$\begin{bmatrix} \dot{z}_1 \\ \dot{z}_2 \\ \vdots \\ \dot{z}_i \\ \vdots \\ \dot{z}_n \end{bmatrix} = \begin{bmatrix} \lambda_1 & & & & & \\ & \lambda_2 & & & & \\ & & \ddots & & & \\ & & & \lambda_i & & \\ & & & & \ddots & \\ & & & & & \lambda_n \end{bmatrix} \begin{bmatrix} z_1 \\ z_2 \\ \vdots \\ z_i \\ \vdots \\ z_n \end{bmatrix} + \begin{bmatrix} \boldsymbol{l}_1\boldsymbol{b}_1 & \boldsymbol{l}_1\boldsymbol{b}_2 & \cdots & \boldsymbol{l}_1\boldsymbol{b}_d \\ \boldsymbol{l}_2\boldsymbol{b}_1 & \boldsymbol{l}_2\boldsymbol{b}_1 & \cdots & \boldsymbol{l}_2\boldsymbol{b}_d \\ \vdots & \vdots & \ddots & \vdots \\ \boldsymbol{l}_i\boldsymbol{b}_1 & \boldsymbol{l}_i\boldsymbol{b}_1 & \cdots & \boldsymbol{l}_i\boldsymbol{b}_d \\ \vdots & \vdots & \ddots & \vdots \\ \boldsymbol{l}_n\boldsymbol{b}_1 & \boldsymbol{l}_n\boldsymbol{b}_1 & \cdots & \boldsymbol{l}_n\boldsymbol{b}_d \end{bmatrix} \begin{bmatrix} u_1 \\ u_2 \\ \vdots \\ u_d \end{bmatrix} \tag{A.4}$$

Single z_i out for discussion

$$\dot{z}_i = \lambda_i z_i + \boldsymbol{l}_i\boldsymbol{b}_1 u_1 + \boldsymbol{l}_i\boldsymbol{b}_1 u_2 + \cdots + \boldsymbol{l}_i\boldsymbol{b}_d u_d \tag{A.5}$$

Assume each elements in u is step input with random amplitude u_q^0, that is

$$u_q(t) = \begin{cases} u_q^0 & t \geq 0, \\ 0 & t < 0. \end{cases} \tag{A.6}$$

Conduct Laplace transform for both sides of (A.5)

$$sz_i(s) - z_i(0) = \lambda_i z_i(s) + \frac{\boldsymbol{l}_i \boldsymbol{b}_1 u_1^0}{s} + \frac{\boldsymbol{l}_i \boldsymbol{b}_1 u_2^0}{s} + \cdots + \frac{\boldsymbol{l}_i \boldsymbol{b}_d u_d^0}{s} \tag{A.7}$$

$$z_i(s) = \frac{z_i(0)}{(s - \lambda_i)} + \frac{\boldsymbol{l}_i \boldsymbol{b}_1 u_1^0}{(s - \lambda_i)s} + \frac{\boldsymbol{l}_i \boldsymbol{b}_1 u_2^0}{(s - \lambda_i)s} + \cdots + \frac{\boldsymbol{l}_i \boldsymbol{b}_d u_d^0}{(s - \lambda_i)s} \tag{A.8}$$

$$\begin{aligned} z_i(s) &= \frac{z_i(0)}{(s - \lambda_i)} + \frac{\boldsymbol{l}_i \boldsymbol{b}_1 u_1^0}{\lambda_i} \frac{1}{s - \lambda_i} - \frac{\boldsymbol{l}_i \boldsymbol{b}_1 u_1^0}{\lambda_i} \frac{1}{s} + \cdots + \frac{\boldsymbol{l}_i \boldsymbol{b}_d u_d^0}{\lambda_i} \frac{1}{s - \lambda_i} - \frac{\boldsymbol{l}_i \boldsymbol{b}_d u_d^0}{\lambda_i} \frac{1}{s} \\ &= \frac{z_i(0)}{(s - \lambda_i)} + \frac{1}{s - \lambda_i} \sum_{q=1}^{d} \frac{\boldsymbol{l}_i \boldsymbol{b}_q u_q^0}{\lambda_i} - \frac{1}{s} \sum_{q=1}^{d} \frac{\boldsymbol{l}_i \boldsymbol{b}_q u_q^0}{\lambda_i} \end{aligned} \tag{A.9}$$

Then conduct inverse Laplace transform

$$z_i(t) = z_i^0 e^{\lambda_i t} + e^{\lambda_i t} \sum_{q=1}^{d} \frac{\boldsymbol{l}_i \boldsymbol{b}_q u_q^0}{\lambda_i} - \sum_{q=1}^{d} \frac{\boldsymbol{l}_i \boldsymbol{b}_q u_q^0}{\lambda_i} \tag{A.10}$$

Recall (A.2), then

$$\boldsymbol{z}(0) = M^{-1} \boldsymbol{x}(0). \tag{A.11}$$

For a specific mode $z_i(0)$,

$$z_i(0) = \boldsymbol{l}_i \boldsymbol{x}(0) \tag{A.12}$$

From (A.3b) and (A.10),

$$\begin{bmatrix} y_1 \\ y_2 \\ \vdots \\ y_k \\ \vdots \\ y_m \end{bmatrix} = \begin{bmatrix} \boldsymbol{c}_1\boldsymbol{r}_1 & \boldsymbol{c}_1\boldsymbol{r}_2 & \cdots & \boldsymbol{c}_1\boldsymbol{r}_n \\ \boldsymbol{c}_2\boldsymbol{r}_1 & \boldsymbol{c}_2\boldsymbol{r}_2 & \cdots & \boldsymbol{c}_2\boldsymbol{r}_n \\ \vdots & \vdots & \ddots & \vdots \\ \boldsymbol{c}_k\boldsymbol{r}_1 & \boldsymbol{c}_k\boldsymbol{r}_2 & \cdots & \boldsymbol{c}_k\boldsymbol{r}_n \\ \vdots & \vdots & \ddots & \vdots \\ \boldsymbol{c}_m\boldsymbol{r}_1 & \boldsymbol{c}_m\boldsymbol{r}_2 & \cdots & \boldsymbol{c}_m\boldsymbol{r}_n \end{bmatrix} \begin{bmatrix} z_1 \\ z_2 \\ \vdots \\ z_i \\ \vdots \\ z_n \end{bmatrix} \tag{A.13}$$

$$\begin{aligned} y_k &= \sum_{i=1}^{n} \boldsymbol{c}_k\boldsymbol{r}_i \left(z_i^0 e^{\lambda_i t} + e^{\lambda_i t} \sum_{q=1}^{d} \frac{\boldsymbol{l}_i \boldsymbol{b}_q u_q^0}{\lambda_i} - \sum_{q=1}^{d} \frac{\boldsymbol{l}_i \boldsymbol{b}_q u_q^0}{\lambda_i} \right) \\ &= \underbrace{\sum_{i=1}^{n} \left[\boldsymbol{c}_k\boldsymbol{r}_i \left(z_i^0 + \sum_{q=1}^{d} \frac{\boldsymbol{l}_i \boldsymbol{b}_q u_q^0}{\lambda_i} \right) e^{\lambda_i t} \right]}_{\text{Exponential Terms}} - \underbrace{\sum_{i=1}^{n} \left[\boldsymbol{c}_k\boldsymbol{r}_i \sum_{q=1}^{d} \frac{\boldsymbol{l}_i \boldsymbol{b}_q u_q^0}{\lambda_i} \right]}_{\text{Constant}} \end{aligned} \tag{A.14}$$

For the exponential terms associating with a pair of complex eigenvalue $\lambda_i = \alpha_i \pm j\beta_i$

$$\boldsymbol{c}_k\boldsymbol{r}_i \left(\boldsymbol{l}_i \boldsymbol{x}_0 + \sum_{q=1}^{d} \frac{\boldsymbol{l}_i \boldsymbol{b}_q u_q^0}{\lambda_i} \right) e^{(\alpha_i + j\beta_i)t} + \boldsymbol{c}_k\bar{\boldsymbol{r}}_i \left(\bar{\boldsymbol{l}}_i \boldsymbol{x}_0 + \sum_{q=1}^{d} \frac{\bar{\boldsymbol{l}}_i \boldsymbol{b}_q u_q^0}{\bar{\lambda}_i} \right) e^{(\alpha_i - j\beta_i)t} \tag{A.15}$$

Let

$$D_i = \boldsymbol{c}_k\boldsymbol{r}_i \left(\boldsymbol{l}_i \boldsymbol{x}_0 + \sum_{q=1}^{d} \frac{\boldsymbol{l}_i \boldsymbol{b}_q u_q^0}{\lambda_i} \right) \tag{A.16}$$

Then (A.15) becomes

$$\begin{aligned} D_i e^{(\alpha_i + j\beta_i)t} + \bar{D}_i e^{(\alpha_i - j\beta_i)t} &= 2e^{\alpha_i t} |D_i| \cos(\beta_i t + \phi_i) \\ &= 2 \left| \boldsymbol{c}_k\boldsymbol{r}_i \left(\boldsymbol{l}_i \boldsymbol{x}_0 + \sum_{q=1}^{d} \frac{\boldsymbol{l}_i \boldsymbol{b}_q u_q^0}{\lambda_i} \right) \right| e^{\alpha_i t} \cos(\beta_i t + \phi_i) \\ &= \underbrace{2 \left| \boldsymbol{c}_k\boldsymbol{r}_i \left(\boldsymbol{l}_i \boldsymbol{x}_0 + \frac{\boldsymbol{l}_i B \boldsymbol{u}_0}{\lambda_i} \right) \right|}_{\text{Initial Amplitude}} e^{\alpha_i t} \cos(\beta_i t + \phi_i) \end{aligned} \tag{A.17}$$

where

$$\phi_i = \tan^{-1} \frac{\mathrm{Im}\left(\boldsymbol{c}_k \boldsymbol{r}_i \left(\boldsymbol{l}_i \boldsymbol{x}_0 + \sum_{q=1}^{d} \frac{\boldsymbol{l}_i \boldsymbol{b}_q u_q^0}{\lambda_i}\right)\right)}{\mathrm{Re}\left(\boldsymbol{c}_k \boldsymbol{r}_i \left(\boldsymbol{l}_i \boldsymbol{x}_0 + \sum_{q=1}^{d} \frac{\boldsymbol{l}_i \boldsymbol{b}_q u_q^0}{\lambda_i}\right)\right)}$$

Plug (A.15) into (A.14), we find (A.14) is a summation of sinusoidal terms for complex eigenvalues, exponential terms for real eigenvalues and constant. So we could define MOPF as

$$p_i^y = E\left(\frac{2\left|\boldsymbol{c}_k \boldsymbol{r}_i \left(\boldsymbol{l}_i \boldsymbol{x}_0 + \frac{\boldsymbol{l}_i B \boldsymbol{u}_0}{\lambda_i}\right)\right|}{\sum_{k=1}^{n} \left|\boldsymbol{c}_k \boldsymbol{r}_k \left(\boldsymbol{l}_k \boldsymbol{x}_0 + \frac{\boldsymbol{l}_k B \boldsymbol{u}_0}{\lambda_k}\right)\right|}\right) \tag{A.18}$$

If all disturbance happens outsides instead of direct on internal state variables, (A.18) reduces to

$$p_i^y = E\left(\frac{2\left|\boldsymbol{c}_k \boldsymbol{r}_i \boldsymbol{l}_i B \boldsymbol{u}_0 \lambda_i^{-1}\right|}{\sum_{k=1}^{n} \left|\boldsymbol{c}_k \boldsymbol{r}_k \boldsymbol{l}_k B \boldsymbol{u}_0 \lambda_k^{-1}\right|}\right) \tag{A.19}$$